Supporting information for

Bioinspired Design of Nanostructured Elastomers with Crosslinked Soft Matrix Grafting on the Oriented Rigid Nanofibers to Mimic Mechanical Properties of Human Skin

Zhongkai Wang,[†] Feng Jiang,[†] Yaqiong Zhang,[†] Yezi You,[†] Zhigang Wang[†,*], and Zhibin Guan[‡,*]

[†]Department of Polymer Science and Engineering, University of Science and Technology of China, Hefei, Anhui Province 230026, P. R. China

[‡]1102 Natural Sciences II, University of California, Irvine, CA 92697-2025

*Address correspondence to: zgwang2@ustc.edu.cn, zguan@uci.edu

Experimental

Materials and characterization. Ionic liquid, 1-allyl-3-methylimidazolium chloride (AMIMCl) and cellulose were dried at 80 °C under vacuum for 24 h before use. Isoprene was purified by passing through a column filled with basic aluminum oxide to remove the inhibitors. All other chemicals were used as received from the suppliers. FTIR spectra were obtained on an EQUIVOX55 (Bruker) FTIR spectrophotometer. The dried samples were mixed with KBr to form pellets. ^{1}H NMR spectrum was taken on a 400MHz Bruker instrument. NMR chemical shifts were reported in standard format as values in ppm relative to the deuterated solvent. The CP/MAS ^{13}C NMR measurements were performed with a Bruker AVANCE AV III 400WB spectrometer operating at 100.6 MHz for ^{13}C. Samples were placed in 4-mm zirconia rotors and

spun at 4 KHz. In the CP/MAS experiments a contact time of 2.0 ms and a recycle delay of 4.0 s were employed. ^{13}C chemical shifts were in ppm relative to an external sample of tetramethylsilane (TMS). Thermal stability of samples was examined on a SDT Q600 instrument with a heating rate of 20 °C/min from 30 to 600 °C under a nitrogen atmosphere. All the samples were dried under vacuum at 70 °C for 24 h prior to TGA measurements. Dynamic mechanical analyses (DMA) were performed by using a TA-Q800 DMA (TA Instruments, USA). The DMA spectra were scanned with a frequency of 10 Hz and a heating rate of 3 ^{o}C/min.

Synthesis of macroinitiator Cell-BiB. As illustrated in Scheme S1 the preparation procedure of macroinitiator **Cell-BiB** is described as follows: 1.5 g cellulose were dispersed in 40 g AMIMCl, the mixture was heated at 80 ^{o}C under permanent stirring until the cellulose was dissolved completely. Then, a transparent solution was obtained by addition of 15 ml DMF as dilute. Then, 5.8 ml 2-bromoisobutyryl bromide was added dropwise under an ice/water bath. When the dropping process was completed, the reaction mixture was left to become warm at room temperature, and allowed to proceed for 36 h. Then the reaction solution was poured into an excess amount of deionized water and white floccules formed. The product was washed thoroughly with water, then filtered and dried under vacuum at 50 ^{o}C, with around 86 % yield. The degree of substitution (DS) is calculated to be 0.98 according to ^{1}H NMR of **Cell-BiB**, and the result is confirmed by mass increase due to acylation.

Synthesis of CBPs. As illustrated in Scheme S2 the preparation procedure for CBP 1 is

described as follows: a solution of 1200 mg (4.0 mmol of Br) Cell-BiB, 4.5 mg (0.02 mmol) $CuBr_2$, 40 μL (0.2 mmol) PMDETA, 8 mL (80 mmol) isoprene, 35 mg (0.2 mmol) ascorbic acid, 8 mL N,N-dimethylformamide, and 8 mL 1,4-dioxane was polymerized at 70 ^{o}C for 48 h. The resulting product was washed with THF to remove the catalyst and residual monomers, and then dried under vacuum, yielding 5.8 g yellow and transparent elastomer.

FTIR and ^{1}H NMR measurements. Figure S2 shows the FTIR spectra for the cellulose and **Cell-BiB** macroinitiator. The stretching vibration at 1741 cm^{-1} indicates that the 2-bromoisobutyl groups are successfully introduced onto cellulose chains. Figure S3 shows the ^{1}H NMR spectrum for Cell-BiB, which also demonstrates the successful synthesis of macroinitiator **Cell-BiB**. The chemical shift at δ=1.6 ppm is due to the methyl protons of 2-bromoisobutyl group.

Solid-state CP/MAS ^{13}C NMR analysis. Homogeneous graft polymerization based on cellulose macroinitiator has been reported.[1] However, homogeneous graft polymerization of isoprene from cellulose backbone chains remains a challenge. Recently, activator regenerated by electron transfer atom transfer radical coupling (ARGET ATRC) was used to couple polymers prepared *via* ATRP.[2] Herein, as illustrated in Scheme S2, we designed one pot homogeneous synthesis of **CBP**s *via* ARGET ATRP and subsequent ARGET ATRC. In the early stage of the reaction, isoprene monomers were grafted from cellulose backbone chains homogeneously *via* ARGET ATRP. When most of the monomer was consumed, ARGET ATRC

took place and inter- and/or intra-molecular carbon-carbon bonds formed at the periphery of the grafted side chains, which led to the formation of **CBP**s. Figure S4 show the solid-state CP/MAS ^{13}C NMR spectra for cellulose, macroinitiator **Cell-BiB**, and **CBP 1**. The chemical shift of carbonyl carbon appears at 171 ppm, and the chemical shift of methyl carbon of 2-bromoisobutyl group appears at 29.5 ppm. The successful synthesis of **CBP**s can be demonstrated by solid-state CP/MAS ^{13}C NMR. The 10, 11, 12, 13, 14 dominate resonances at 134.8, 125.3, 32.5, 26.7, and 23.6 ppm, respectively, are related to the five carbon atoms of isoprene chain elements. The degree of coupling (DC_{NMR}) of the initiation points was calculated from a ratio of the integrals of NMR peaks using Formula 1 as follows:

$$DC_{NMR} = \frac{S_{9'} - S_{8'}}{S_{9'}} \qquad (1)$$

where $S_{8'}$ and $S_{9'}$ are the integration intensities of the corresponding quaternary carbons and carbonyl carbons of the 2-bromoisobutyryl groups, respectively. According to the solid-state CP/MAS ^{13}C NMR spectrum of **CBP** 1 (Figure S4), the integration intensity of peak S9′ was 1.0 and the integration intensity of peak S8′ was 0.72, and the degree of coupling was calculated to be 0.28. Thus, we estimate that about 28 % of the propagating polyisoprene chains were coupled *via* ARGET ATRC.

TGA analysis. Thermal stability is one of the most important limiting factors for the application of polymeric materials. Figure S5 shows the TGA curves of cellulose, macroinitiator **Cell-BiB**, **CBP 1**, and polyisoprene at a heating rate of 20 °C/min under nitrogen atmosphere. The maximum degradation of cellulose occurs at 367 ^{o}C. Thermal stability of

macroinitiator **Cell-BiB** decreases significantly as confirmed from its maximum degradation temperature at 267 ^{o}C if compared with cellulose, which results from the introduction of relatively unstable 2-bromoisobutyl groups. TGA curve for **CBP 1** shows two maximum decompositions, which are comparable to that of **Cell-BiB** and polyisoprene, respectively, and implies that the cellulose backbone chains have been successfully wrapped by polyisoprene side chains.

Cyclic tensile deformation treatment. In order to reconfigure the microstructure of **CBP**s, cyclic tensile deformation processing was carried out using a Linkam TST 350 tensile deformation test machine at room temperature. Each sample of **CBP**s was cut into dog-bone shape specimen with thickness of about 1 mm. The cyclic tensile deformation treatment was conducted stepwise to progressively higher tensile strains with the strain rate fixed at 10 %/min. In each step, once the sample reached the appropriate tensile strain, the crosshead direction was reversed and the sample strain was decreased at the same nominal strain rate until zero stress was achieved. Once the stress was fully released, the crosshead was immediately reversed, and the sample was then extended again at the same constant strain rate until it reached the next targeted maximum strain. The cyclic deformation treatment was continued until in the final cycle the targeted final strain was reached.

Microstructure analyses. Synchrotron SAXS and WAXD measurements were performed to characterize the microstructures of **CBP** samples during tensile deformation. Synchrotron SAXS measurements were performed at SSRF, Shanghai, China. The wavelength of the X-ray

radiation was 0.124 nm, and the sample-to-detector distance was 2417 mm. Wide angle X-ray diffraction (WAXD) measurements were carried out at X-ray Diffraction and Scattering Beamline (U7B), National Synchrotron Radiation Laboratory (NSRL) in Hefei, China. The wavelength used was 0.154 nm. Real-time SAXS and WAXD measurements were carried out during tensile deformation using a Linkam TST 350 tensile deformation test machine that was available at the beamlines. Low temperature ultrathin sections (90 nm) were cut on a Leica EM Fc6 ultramicrotome and the TEM observations were performed on a JEM-2010 conventional TEM operating at 120 KV. The polyisoprene matrix was stained by vapour of osmium tetraoxide (OsO_4) solution of 1 % before TEM imaging. Figure S7 shows 1D SAXS intensity profiles by azimuthal averaging from 80° to 100° and from 170° to 190°, respectively, for **CBP 1** during cyclic tensile deformation shown in Figure 3a and during tensile deformation shown in Figure 3b. We can conclude that the inter-domain space along the tensile direction of **CBP 1** increases. Figure S8 shows the SAXS azimuthal intensity profiles for **CBP 1** during cyclic tensile deformation shown in Figure 3a and during tensile deformation shown in Figure 3b. It can be seen that an isotropic diffuse scattering intensity appears for the undeformed **CBP 1**. With the strain increased the scattering peaks can be clearly observed. Accordingly we confirm that during cyclic tensile deformation the cellulose nanospheres change into cellulose nanofibers. Figure S9 shows the 1D WAXD intensity profiles for **CBP 1** during cyclic tensile deformation shown in Figure 3a and during tensile deformation shown in Figure 3b. This result indicates that no crystalline structures form during the tensile deformation. Figure S10 shows the WAXD azimuthal intensity profiles for **CBP 1** during cyclic tensile deformation shown in

Figure 3a and during tensile deformation shown in Figure 3b. The undeformed **CBP 1** exhibits predominantly isotropic diffraction pattern. As the extension ratio increases, the weak azimuthal peaks appear on the equator, indicating that the amorphous chain segments are slightly oriented along the tensile deformation direction.

Tensile mechanical properties. The mechanical properties of **CBP**s after cyclic tensile deformation were measured using a Linkam TST 350 tensile deformation test machine. The specimens were extended at the strain rate of 72 %/min at room temperature. Each measurement was repeated at least three times. In order to lower the initial elastic modulus, we used mineral oil to plasticize **CBP**s. **CBP 1-5** samples were immersed in mineral oil at 70 ^{o}C under vacuum for 40 to 120 min, and the mineral oil mass content was controlled to be 20 wt%. **CBP 1-5** samples containing mineral oil are defined as **CBP 1-5M**. Table S2 summarizes the mechanical properties of all **CBP** samples as well as different types of human skin reported in the literature. Figure S11 shows the nominal stress-nominal strain curve during the cyclic tensile deformation with maximum strains of 10 %, 20 %, 30 % and so on up to 65 % for **CBP 1** sample after the first series of cyclic deformation shown in Figure 3a. The elastic recovery at zero stress after cyclic tensile deformation can be calculated using Formula 2 as follows:

$$\text{Elastic recovery} = \frac{\varepsilon_{\max} - \varepsilon_{\max,0}}{\varepsilon_{\max}} \qquad (2)$$

where $\varepsilon_{\max}$ and $\varepsilon_{\max,0}$ are the maximum strain and the strain in the cycle at zero stress after the maximum strain $\varepsilon_{\max}$, respectively. Figure S12 shows the changes of elastic recovery with maximum strain in each cyclic step for **CBP 1-5** after one series of cyclic deformation. We can

conclude that the elastic recoveries of **CBP 1-5** are comparable to that of human skin after the cyclic tensile deformation processing.

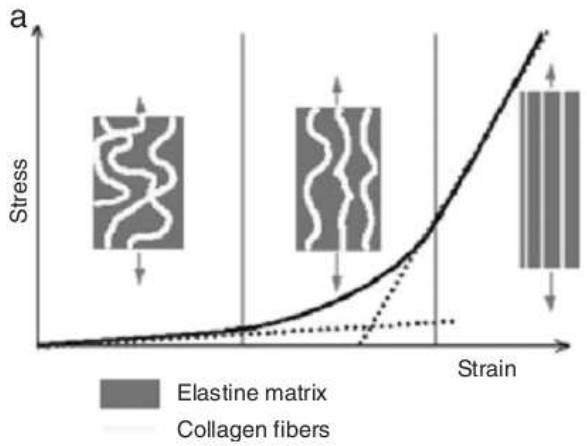

Figure S1. Nonlinear elasticity due to the orientation of collagen fibers. Inset are the corresponding microstructure models.[3]

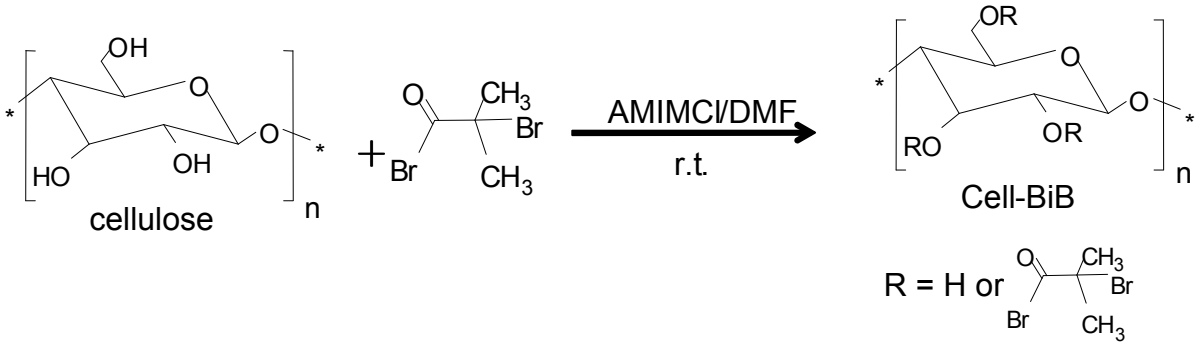

Scheme S1. Synthesis of macroinitiator **Cell-BiB**.

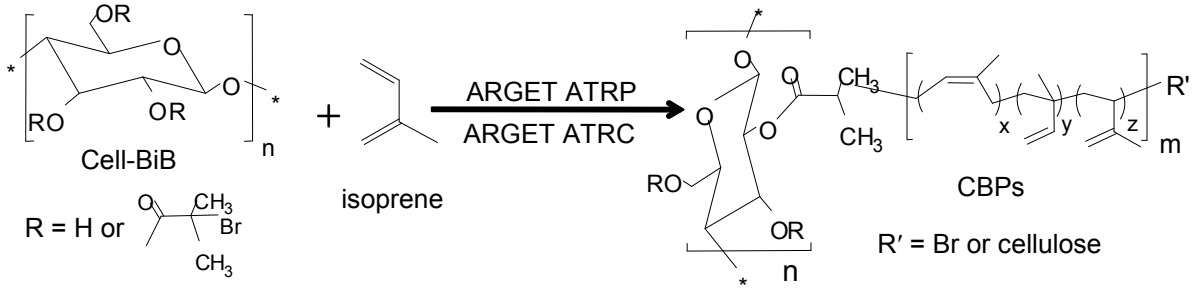

Scheme S2. Synthesis of cross-linked brush biocopolymers (**CBP**s).

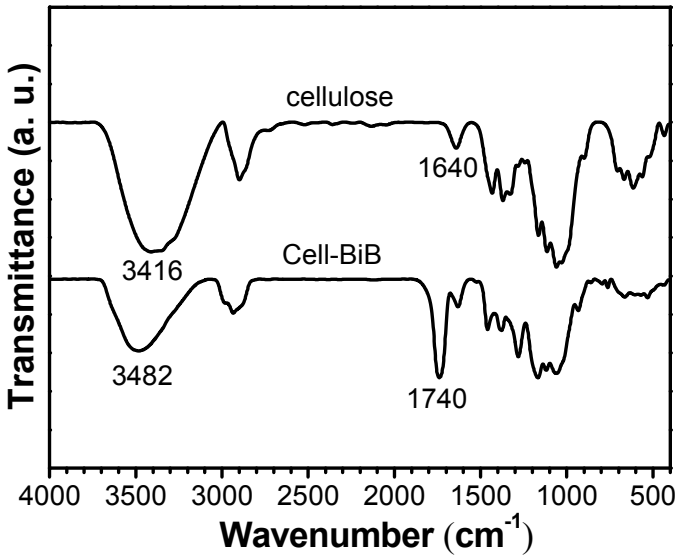

Figure S2. FTIR spectra of cellulose and macroinitiator **Cell-BiB**.

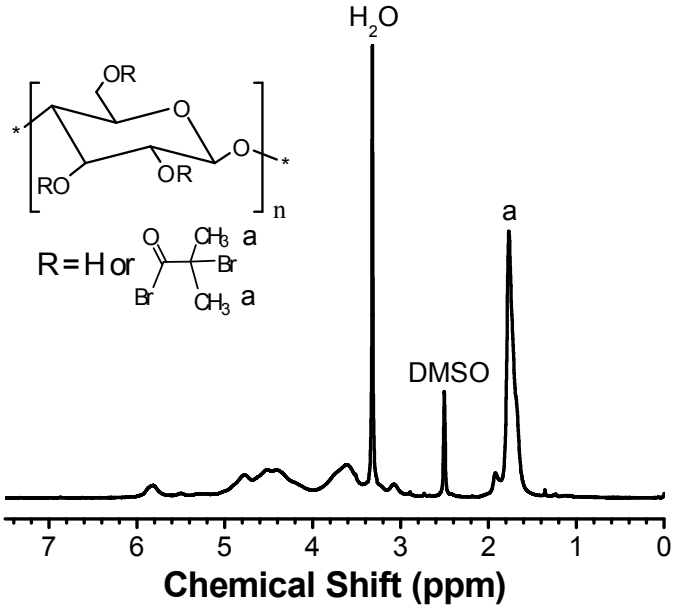

Figure S3. ^{1}H NMR spectrum of macroinitiator **Cell-BiB**.

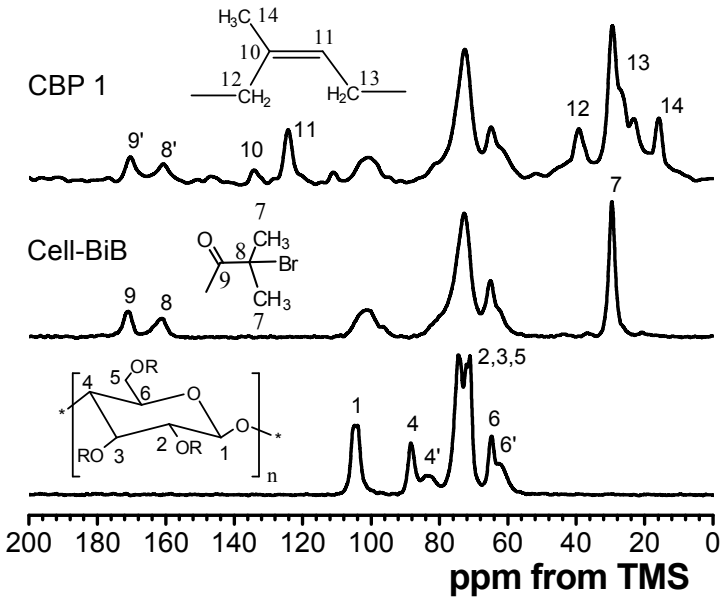

Figure S4. Solid-state CP/MAS ^{13}C NMR spectra of cellulose, **Cell-BiB** and **CPB 1**.

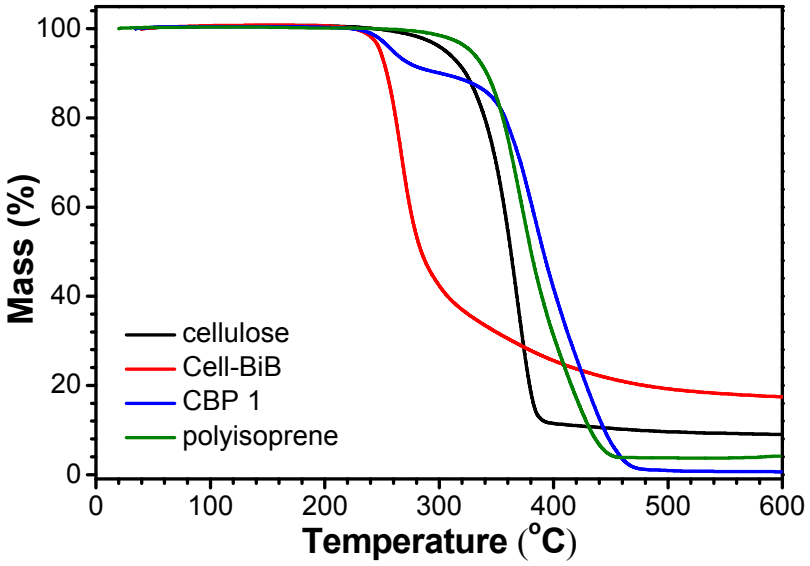

Figure S5. TGA curves of cellulose, **Cell-BiB**, **CBP 1**, and polyisoprene.

Table S1. Glass transition temperatures (T_gs) of CBP 1-5 obtained from DMA.

Sample code	Cellulose content (wt %)	T_g of cellulose (^oC)	T_g of PI (^oC)
CBP 1	20.6	184	-39
CBP 2	14.3	164	-38
CBP 3	8.7	143	-31
CBP 4	6.0	123	-32
CBP 5	4.3	64	-32

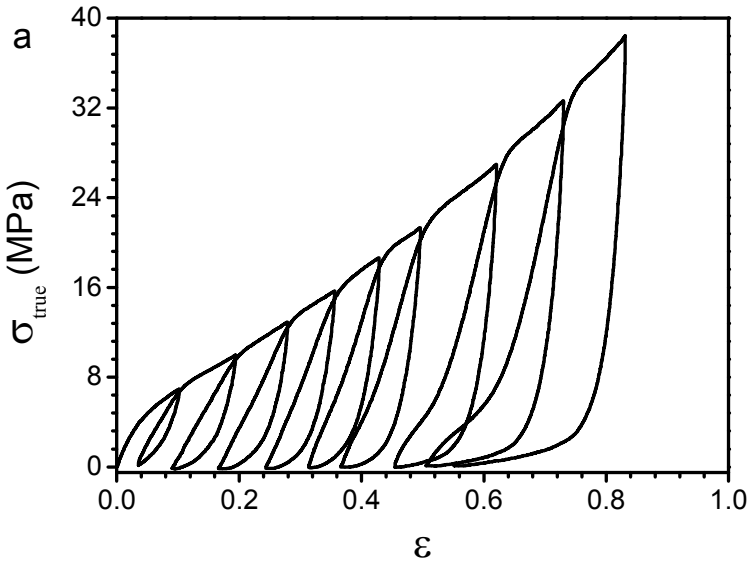

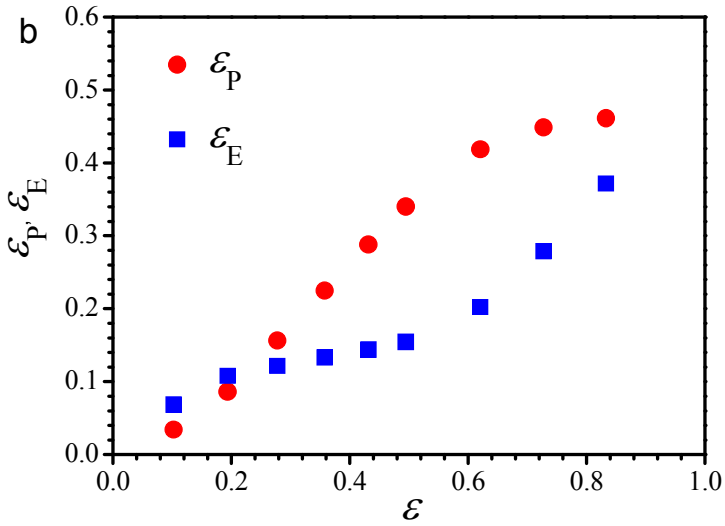

Figure S6. a) True stress *versus* true strain curves for **CBP 1** during the cyclic deformation series in Figure 3a. (b) Dependences of the elastic true strain, ε_E (remaining strain at zero load) and plastic true strain, ε_P (recovered strain after unloading) on the maximal true strain, ε, for **CBP 1.** The data are derived from Figure S6a.

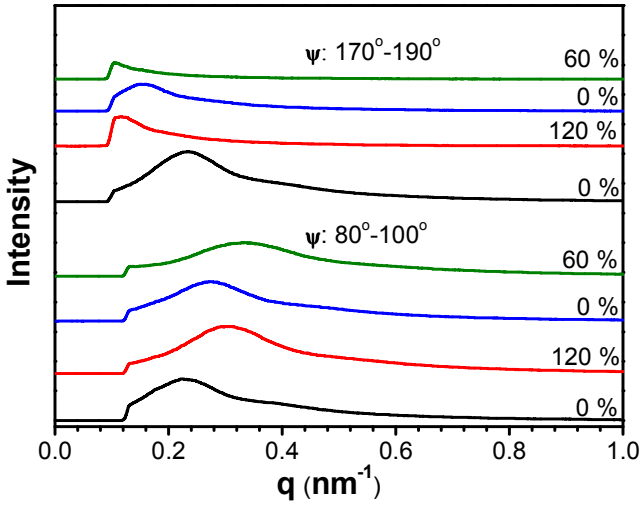

Figure S7. 1D SAXS intensity profiles by azimuthal averaging from 80° to 100° and from 170° to 190°, respectively, for **CBP 1** during cyclic tensile deformation shown in Figure 3a (black

and red lines) and during tensile deformation shown in Figure 3b (blue and olive lines).

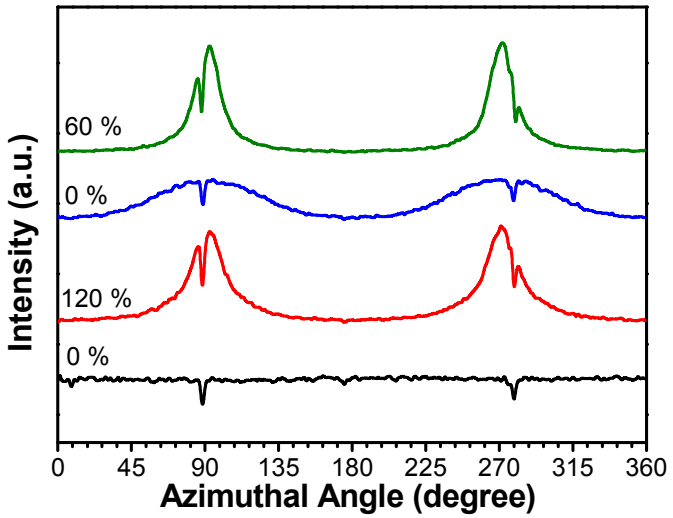

Figure S8. SAXS azimuthal intensity profiles for **CBP 1** during cyclic tensile deformation shown in Figure 3a (black and red lines) and during tensile deformation shown in Figure 3b (blue and olive lines).

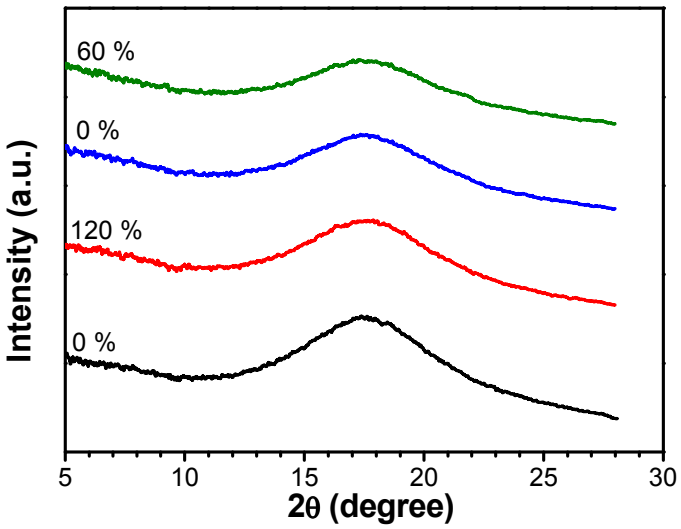

Figure S9. 1D WAXD intensity profiles for **CBP 1** during cyclic tensile deformation shown in Figure 3a (black and red lines) and during tensile deformation shown in Figure 3b (blue and

olive lines).

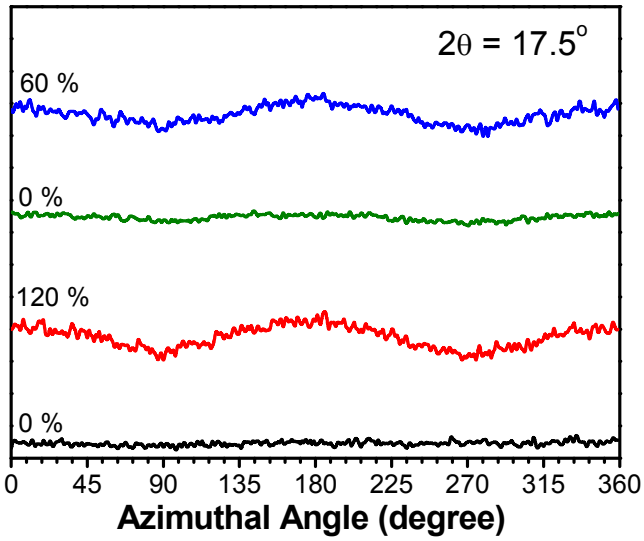

Figure S10. WAXD azimuthal intensity profiles for **CBP 1** during cyclic tensile deformation shown in Figure 3a (black and red lines) and during tensile deformation shown in Figure 3b (blue and olive lines).

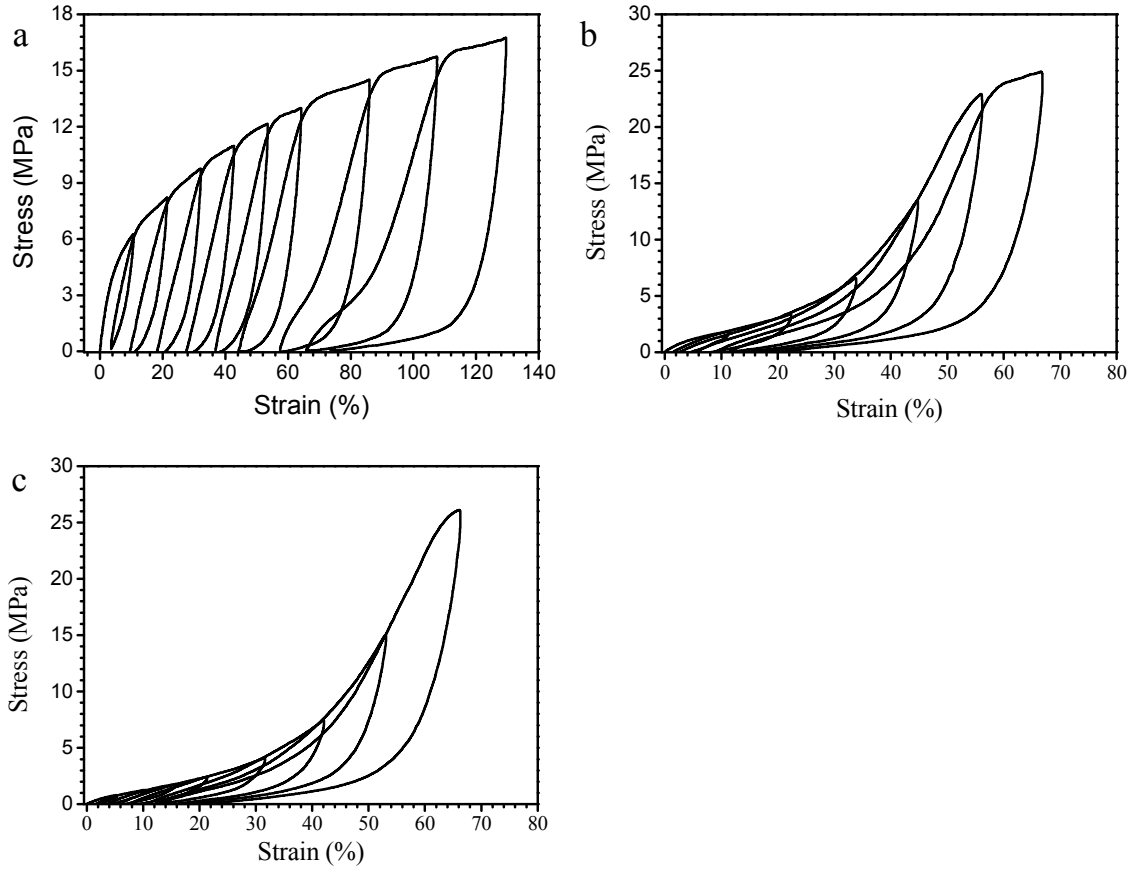

Figure S11. Nominal stress-nominal strain curves of **CBP1** during the first series of cyclic deformation (a), the second series of cyclic deformation (b), and the third series of cyclic deformation (c). The strain rate was 10 %/min.

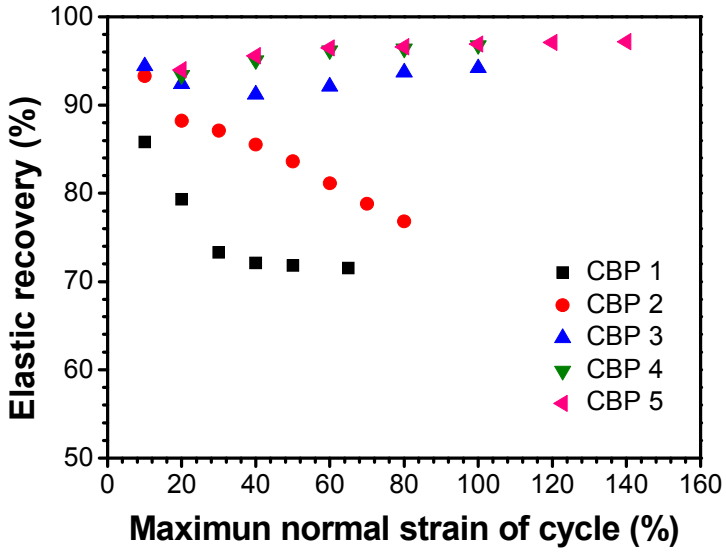

Figure S12. Changes of elastic recovery with maximum strain in each cyclic step for **CBP 1-5** after one series of cyclic deformation.

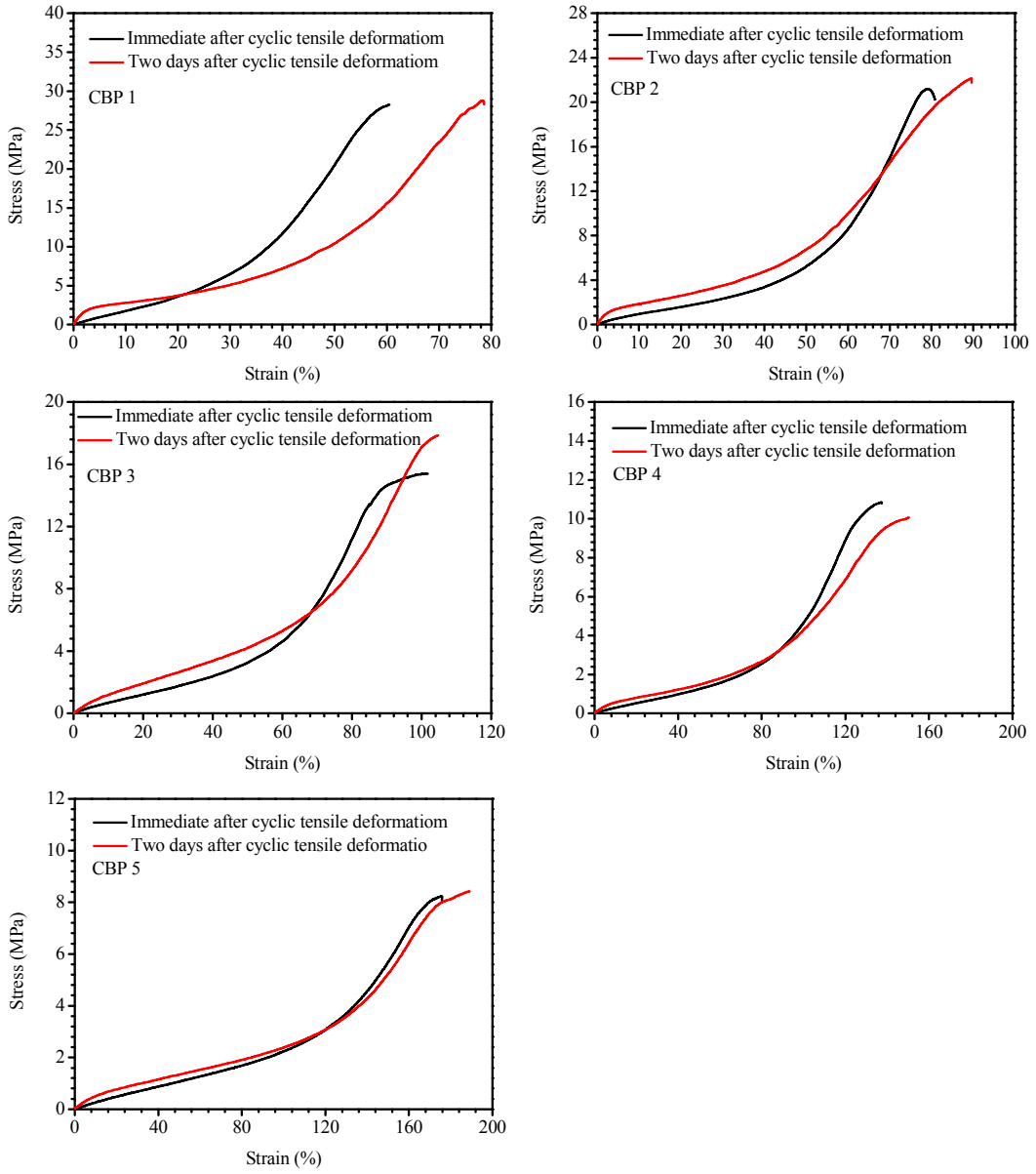

Figure S13. Stress-strain curves for **CPB 1-5** obtained immediate after the cyclic tensile deformation and then after relaxed for two days, respectively.

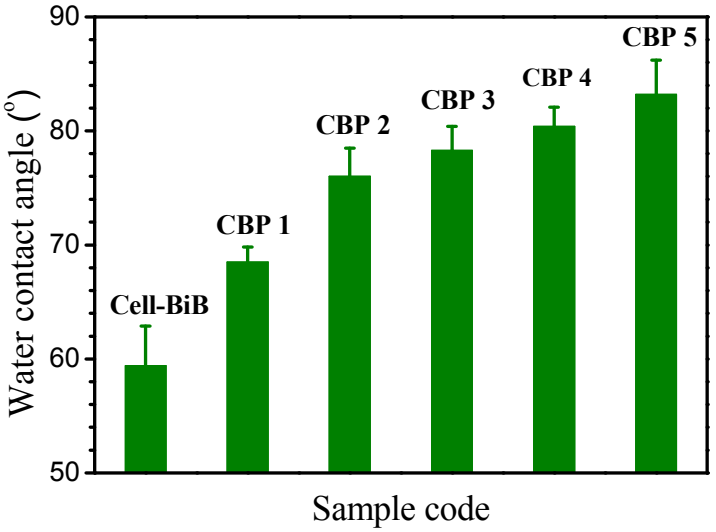

Figure S14. Water contact angles measured at room temperature for Cell-BiB and CBP 1-5.

Table S2. Mechanical properties of **CBP**s as well as of different types of human skin

Sample code	UTS[a] (MPa)	Failure strain[b] (%)	Initial elastic modulus[c] (MPa)	Final elastic modulus[d] (MPa)
		Human skin		
Human skin[4]	1–24	17–207	0.69–3.7	2.9–54.0
Human skin[5]	5–32	30–115	N/A	15–150
Human skin[6]	5.7–12.6	27–59	N/A	19.5–87.1
Human skin[7]	N/A	54 ± 17	1.18 ± 0.88	83.3 ± 34.9
		CBPs		
CBP 1	34.3 ± 2.3	53 ± 7	11.3 ± 0.6	142.5 ± 4.6
CBP 2	25.5 ± 2.0	76 ± 8	6.6 ± 0.9	107.9 ± 6.4
CBP 3	17.6 ± 1.3	90 ± 10	3.7 ± 0.3	65.7 ± 2.5
CBP 4	12.4 ± 0.4	120 ± 17	2.6 ± 0.2	34.2 ± 4.6
CBP 5	9.7 ± 0.5	166 ± 13	2.1 ± 0.3	18.0 ± 1.2
		CBPs containing 20 wt% mineral oil		
CBP 1M	19.0 ± 1.7	58 ± 8	4.4 ± 0.6	68.9 ± 6.2
CBP 2M	15.8 ± 1.3	76 ± 4	3.4 ± 0.2	57.8 ± 4.7
CBP 3M	13.0 ± 0.5	98 ± 11	3.0 ± 0.4	25.2 ± 2.9
CBP 4M	11.3 ± 1.0	125 ± 17	2.5 ± 0.6	28.7 ± 3.1
CBP 5M	7.7 ± 0.4	165 ± 19	1.9 ± 0.4	15.2 ± 0.9

[a]UTS represents the ultimate tensile strength. [b]The failure strain is the maximum strain obtained before failure. [c]The initial elastic modulus is the slope of the stress-strain curve at the low strain. [d]The final elastic modulus is defined as the slope of the linear portion of the stress-strain curve at the high strain. The tensile measurements were all performed at the strain rate of 72 %/min.

References

(1) T. Meng, X. Gao, J. Zhang, J. Yuan, Y. Zhang, J. He, *Polymer* **2009**, *50*, 447.

(2) K. M. Domingues, E. S. Tillman, *J Polym Sci, Part A: Polym. Chem.* **2010**, *48*, 5737.

(3) Delalleau, A.; Josse, G.; Lagarde, J. M.; Zahouani, H.; Bergheau, J. M. *Skin Res. Technol.* **2008**, *14*, 152.

(4) L. Jansen, P. Rottier, *Dermatology* **2009**, *117*, 65.

(5) H. Vogel, *Bioengineering and the skin* **1987**, *3*, 67.

(6) C. Jacquemoud, K. Bruyere-Garnier, M. Coret, *J. Biomech.* **2007**, *40*, 468.

(7) A. Ní Annaidh, K. Bruyère, M. Destrade, M. D. Gilchrist, M. Otténio, *J. Mech. Behav. Biomed.* **2012**, *5*, 139.